An improved PaSR-based soot model for turbulent fires

C J Wang[a]，*H R Liu*[a] *and J X Wen*[b,1]

[a]*School of Civil Engineering, Hefei University of Technology, Hefei, 230009, Anhui, China*

[b]*Warwick FIRE, School of Engineering, University of Warwick, Coventry CV4 7AL, UK*

Abstract

The extension of the laminar smoke point based approach to turbulent combustion using the partially stirred reactor (PaSR) concept proposed by Chen et al. [24,25] has been further improved to overcome the limitation in the formulations of Chen et al. [24,25] which assumed infinitely fast soot oxidation chemistry and constant soot formation characteristic time. In the PaSR approach, each computational cell is split into two zones: the reacting zone and the non-reacting zone. Soot formation and oxidation are assumed to take place at finite rates in the reacting zone and computed from the corresponding laminar rates and the mass fractions for soot formation and oxidation, which are evaluated in each computational cell from the characteristic time scales for turbulent mixing, soot formation and oxidation. Since soot would be produced in not only the fine structures but also surrounding fluids in the Eddy-Dissipation-Concept (EDC) model，the average field parameters between the fine structure and surrounding fluid are employed instead of those Favre-averaged values in Chen et al.'s soot formation model. The newly extended model has been implemented in FireFOAM, a large eddy simulation (LES) based solver for fire simulation based on the open source CFD code OpenFOAM®. Numerical simulations of a 30 cm diameter heptane and toluene pool fires tested by Klassen and Gore [29] were performed for validation. The predicted soot volume fraction and temperature have achieved improved agreement with the experimental measurements in comparison with that of Chen et al. [24, 25], demonstrating the potential of the improved PaSR-based soot model for fire applications.

[1] *Correspondence Jennifer.wen@warwick.ac.uk*

Keywords: Turbulent pool fire; Partially Stirred Reactor; Smoke Point Soot Model; Large Eddy Simulation; FireFOAM

Nomenclatures		$\widetilde{Y}_s$	soot mass fraction
A_0	pre-exponential factor	Z	mixture fraction
A_{Lsp}	fuel-independent constant	$Z_{S,0}$	critical mixture fractions for soot oxidation
A_S	soot particulate surface area	$Z_{S,f}$	critical mixture fractions for soot formation
b	stoichiometric oxygen-fuel ratio	Z_{st}	stoichiometric mixture fraction
C_p	specific heat	**Greek symbols**	
C_{SP}	constant	ρ	density
D	laminar diffusion coefficient	ν_t	turbulent kinematic viscosity coefficient
D^*	characteristic plume length scale	$\overline{\omega}_s$	filtered soot source term
E_{a_0}	activation energy for soot oxidation	$\omega_{S,f}$	laminar soot formation rate
f_v	soot volume fraction	$\omega_{S,O}$	laminar soot formation rate
g	gravity acceleration	γ	exponent for temperature
H	height	$\psi_{S,f}$	constant
k	total turbulent kinetic energy	$\psi_{S,O}$	constant
LSP	smoke point height	$\kappa_{S,f}$	mass fraction of the reacting part for soot formation
$\dot{m}^*$	mass transfer per unit of mass of the fine structure region	$\kappa_{S,O}$	mass fraction of the reacting part for soot oxidation
$\overline{p}$	Favre- averaged pressure	$\tau_{S,f,c}$	characteristic time for soot formation
Pr_t	turbulent Prandtl number	$\tau_{S,O,c}$	characteristic time for soot oxidation
Q	heat release rate	τ_{mix}	Characteristic time for turbulent mixing
T	activation temperature	ν	kinematic viscosity coefficient
T_0	activation temperature	κ_s	soot absorption coefficient
T_∞	ambient air temperature	ε	dissipation rate
T_{Sur}	Temperature in surround fluid	γ^*	mass fraction of the fine structures
T^*	temperature in fine structures	χ	reacting fraction of the fine structures
u	velocity	ρ_∞	ambient air density
W_k	atomic weight for element k	**Subscripts**	
Y^*	species mass fraction in fine structures	F	fuel stream
Y_{fu}	fuel mass fraction	**Superscripts**	

Y_{fu}^0	fuel mass fraction in the fuel stream	I	values at the inlet
$\hat{Y}_k$	elemental mass fraction	∞	values under ambient condition
Y_{O_2}	oxygen mass fraction	C	carbon
$Y_{O_2}^0$	ambient oxygen mass fraction	H	hydrogen
Y_{Sur}	species mass fraction in surround fluid	O	oxygen

1. Introduction

Soot and thermal radiation are two key factors affecting fire hazards. Soot particulates together with carbon dioxide and water vapour etc. are the main components of fire smoke, which decreases visibility. On the other hand, soot is the main contributor to thermal radiation from hydrocarbon fires; but for very large hydrocarbon fires, smoke shielding also has the effect of blocking the emitted flame radiation from escaping out to the surroundings [1-5]. Accurate prediction of soot formation and oxidation is hence of considerable importance to fire hazards analysis.

The complexity of soot formation chemistry is related to its nucleation, inception, coagulation and agglomeration. Detailed soot chemistry models [6-9] were previously developed to cater for all these underlying physics. However, they are computationally expensive and impractical for use in fire safety engineering. Various empirical soot models developed up to date either directly use experimental measurements [10,11] or indirectly employ experimental measurements for parameter calibration [12]. But as commented by Lautenberger [13], the empirical models are only suitable for special fuel, oxidation and pressure conditions which were covered in the test data used for their derivation. Model constants determined from tests of certain fuel and burning conditions cannot be applied to other fuel and conditions. A better choice is hence the semi-empirical models which are a compromise of the above two approaches and can be extended to a wide variety of fuels and applied to most fire sceneries with acceptable computational cost. Such semi-empirical models should also avoid both detailed soot chemistry and the calculations of soot particle number density and its surface area.

The potential of a smoke point based model to alleviate these limitations of the empirical models were recognized by Markstein and De Ris [14] in the 1980s. The concept was further elaborated by Delichatsios [15] who derived a global soot formation rate based on the experiemental analysis and concluded that the soot propensity of a fuel is inversely proportional to its laminar smoke point (LSP) height. Lautenberger et al. [16] related the peak soot formation rate to LSP and modeled soot oxidation as a surface area independent process. Beji et al. [17,18] employed an Arrhenius reaction rate for soot formation by considering a temperature exponent and an activation temperature in combination with a constant soot oxidation rate of 1 $kg/m^3.s^{-1}$. Their work was further continued by Yao et al. [19] who used the soot oxidation model of Lindstedt and co-workers[20, 21] to remove the emipirically suggested constant by Beji et al. [17,18]. Although promising, the applicability of the LSP approach to fires, which are buoyancy-driven and generally turbulent, depends on its extension from laminar to the turbulent regime. Yao et al. [19,22] adopted the conditional moment closure (CMC) and Alternative Conditional Source-term Estimation (A-CSE) approaches to treat the soot source term in turbulent pool fires, but their model requires solution of the integrated equations to obtain the conditional scalars and is computationally expensive. Chatterjee et al. [23] proposed a "radiatively perturbed laminar flamelet" concept to account for turbulent soot formation and oxidation, which appears promising but its wide application is hindered by the optically thin assumption during the construction of the lookup table. Chen et al. [24,25] extended the laminar smoke point based soot model to turbulent combustion using the Partially-Stirred-Reactor (PaSR) concept, but assumed infinitely fast soot oxidation chemistry and constant soot formation characteristic time.

In the present study, three significant modifications have been introduced to the PaSR based soot model proposed by Chen et al. [24, 25]: (1) The PaSR concept is used for both turbulent soot formation and oxidation while Chen et al. [24, 25] used the PaSR concept for turbulent soot formation and the EDC concept for turbulent soot oxidation; (2) the finite value of the laminar soot oxidation rate is computed with an established formula [20,21,26]; (3) Instead of fixing the characteristic time for soot

formation as a constant which is non-physical, new formulas are proposed to compute it together with the characteristic time for soot oxidation, based on the time-and-space dependent characteristic time; and (4) the average parameters between the fine structure and surrounding fluid in the EDC model are employed instead of those Favre- averaged values. The new model gives due consideration to the essential physics of soot formation and oxidation while maintaining simplicity and computational efficiency. The new model has been implemented in an in-house version [24-25] of the FireFOAM code [27], a large eddy simulation (LES) based solver for fire simulation within the open source CFD code OpenFOAM® Toolbox [28]. For validation, the 30 cm diameter heptane and toluene pool fires tested by Klassen and Gore [29] have been simulated.

2. Soot Model

For turbulent flames, a spatial filtering soot transport equation [24, 25] are expressed as

$$\frac{\partial \overline{\rho}\widetilde{Y}_s}{\partial t}+\frac{\partial \overline{\rho}\widetilde{u}_j\widetilde{Y}_s}{\partial x_j}=\frac{\partial}{\partial x_j}\left[\overline{\rho}\left(D+\frac{\nu_t}{\mathrm{Pr}_t}\right)\frac{\partial \widetilde{Y}_s}{\partial x_j}\right]+\overline{\omega}_s \tag{1}$$

where u, ρ and $\widetilde{Y}_s$ are the velocity, density and soot mass fraction, respectively. D, ν_t, Pr_t denote laminar diffusion coefficient, turbulent kinematic viscosity, and turbulent Prandtl number. The filtered soot source term, $\overline{\omega}_s$ is computed as the difference of soot formation and oxidation rates,

$$\overline{\omega}_s=\overline{\omega}_{sf}-\overline{\omega}_{so} \tag{2}$$

2.1 Laminar Soot Formation

Based on the LSP concept, the global soot formation model was originally proposed by Delichatsios [15], further developed by Beji et al.[17] and applied to fire simulations by Yao et al. [19] and Chen et al. [24, 25]. The laminar soot formation rate ($\omega_{S,f}$) can be expressed as follows:

$$\begin{cases} \omega_{S,f} = \dfrac{A_{LSP}}{LSP}\rho^2\left(Y_{fu}^0\dfrac{Z-Z_{st}}{1-Z_{st}}\right)\mathrm{T}^{\gamma}e^{\left(-\frac{T_0}{T}\right)}\ \left(\mathrm{kg/m^3/s}\right) & \mathrm{Z_{S,O}} \le \mathrm{Z} \le \mathrm{Z_{S,f}} \\ 0 & \text{else} \end{cases} \tag{3}$$

where A_{LSP} is fuel-independent constant, chosen as $4.4e^{-6}$. The exponent for temperature $\gamma = 2.25$ and activation temperature $T_0 = 2000K$ are specified following Beji et al. [17]. Y_{fu}^0, Lsp and T are the fuel mass fraction in the fuel stream, smoke point height and temperature, respectively. Z is the mixture fraction, expressed as

$$\mathrm{Z} = \frac{bY_{\mathrm{fu}} - Y_{O_2} + Y_{O_2}^0}{bY_{fu}^0 + Y_{O_2}^0} \tag{4}$$

where $Y_{O_2}^0$ and b denote ambient oxygen mass fraction and b is the stoichiometric oxygen-fuel ratio. Y_{fu} and Y_{O_2} are the mass fractions of fuel and oxygen. The stoichiometric mixture fraction $\mathrm{Z_{st}}$ can be expressed as

$$\mathrm{Z_{st}} = \frac{Y_{O_2}^0}{bY_{fu}^0 + Y_{O_2}^0} \tag{5}$$

$\mathrm{Z_{S,f}}$ and $\mathrm{Z_{S,0}}$ are critical mixture fractions for soot formation and oxidation, respectively. They could be normalized by the stoichiometric mixture fraction ($\mathrm{Z_{st}}$) [16, 18]:

$$\mathrm{Z_{S,f}} = \psi_{S,f} Z_{st} \tag{6}$$

$$\mathrm{Z_{S,O}} = \psi_{S,O} Z_{st} \tag{7}$$

where $\psi_{S,f}$ and $\psi_{S,O}$ are assumed as fuel-independent constants, chosen as 2.5 and 1 following Beji et al. [18], respectively.

2.2 Laminar Soot Oxidation

In the model of Chen et al. [24, 25], laminar soot oxidation is assumed to be infinitely fast. This is an acceptable assumption only when the turbulent mixing is relatively slow. The actual soot oxidation rate is finite and dependent on its surface area. Following previous researchers [19-21,26], the following expression is used instead:

$$\begin{cases} \omega_{S,O} = -A_O \mathrm{Y_{O_2}} \mathrm{T}^{0.5} \mathrm{e}^{\left(\frac{\mathrm{E_{a_0}}}{\mathrm{RT}}\right)} \rho \mathrm{Y_S} \mathrm{A_S} & \left(\mathrm{kg/m^3}/s\right) \qquad 0 \le \mathrm{Z} \le \mathrm{Z_{S,O}} \text{ and } \mathrm{T} \ge 1300\,\mathrm{K} \\ 0 & \text{else} \end{cases} \tag{8}$$

where $A_O = 120$ [21], $E_{a_0} = 163540 J/mol$ and $A_S = 160 m^2/g$ [19] are the pre-exponential factor, activation energy for soot oxidation and soot particulate surface area, respectively.

2.3 Turbulent Soot Formation and Oxidation

As described by Chen et al. [24, 25], the Partially Stirred Reactor (PaSR) concept [30-32] is adopted as the basis of their extension of LSP to turbulent combustion. In the PaSR approach, each computational cell is split into two zones. All reactions occur in the reacting part while there is no reaction in the non-reacting zone. The composition in the non-reacting part changes due to mass exchange with the reacting part through turbulent diffusion. The reacting part is treated as a perfectly stirred reactor (PSR), in which all species are assumed to be perfectly mixed with each other and no turbulence is involved. It is assumed that the laminar soot formation and oxidation occur only in the reacting part and soot turbulent transportation takes place between the reacting and non-reacting parts in a cell. Following the PaSR concept, the filtered soot formation rate in the LES framework can be expressed as:

$$\begin{cases} \overline{\omega}_{S,f} = \kappa_{S,f} \omega_{sf}\left(\hat{\mathrm{Y}}_{\mathrm{fu}}, \hat{\mathrm{Y}}_{O_2}, \hat{T}, \hat{\rho}\right) \\ \overline{\omega}_{S,O} = \kappa_{S,O} \omega_{so}\left(\hat{\mathrm{Y}}_{\mathrm{S}}, \hat{\mathrm{Y}}_{O_2}, \hat{T}, \hat{\rho}\right) \end{cases} \tag{9}$$

where $\kappa_{S,f}$ and $\kappa_{S,O}$ can be regarded as the mass fractions of the reacting part for soot formation and oxidation in a cell and expressed as

$$\kappa_{S,f} = \frac{\tau_{S,f,c}}{\tau_{S,f,c} + \tau_{mix}} \tag{10}$$

$$\kappa_{S,O} = \frac{\tau_{S,O,c}}{\tau_{S,O,c} + \tau_{mix}} \tag{11}$$

where $\tau_{S,f,c}$ and $\tau_{S,O,c}$ are the characteristic time for soot formation and oxidation respectively. Chen et al. [24, 25] directly related $\tau_{S,f,c}$ with laminar smoke point height as $\tau_{S,f,c} = C_{SP} \cdot LSP$, and assumed that C_{SP} is a constant. Based on a previous finding that $\tau_{S,f,c}$ is a constant value of 40 ms for laminar ethylene diffusion flame [33], they obtained $C_{SP} = \frac{\tau_{S,f,c,ethylene}}{LSP_{ethylene}} = 0.377 s/m$ and further assumed that $\tau_{S,f,c}$ is a constant for one specified gas everywhere. In reality, C_{SP} may be not a constant for any laminar flame and $\tau_{S,f,c}$ is determined by local fuel concentration and soot formation rate; and hence varies with space location. The situation for $\tau_{S,O,c}$ is also similar, and it is determined by local soot concentration, oxygen concentration and soot oxidation rate. According to the definition of chemical reaction characteristic time, it is hence proposed that $\tau_{S,f,c}$ and $\tau_{S,O,c}$ can be expressed as

$$\begin{cases} \tau_{\mathrm{S,f,c}} = \dfrac{\overline{\rho}\hat{Y}_{fu}}{\omega_{s,f}} \\ \tau_{\mathrm{S,O,c}} = \min\left(\dfrac{\overline{\rho}\hat{Y}_S}{\omega_{S,O}}, \dfrac{\overline{\rho}\hat{Y}_{O_2}}{b\omega_{S,O}}\right) \end{cases} \tag{12}$$

The characteristic time for turbulent mixing τ_{mix} can be calculated as the geometric mean of the Kolmogorov and Taylor length scales, which was firstly suggested by Karlsson and Chomiak [34,35] . Chen et al.[24, 25] employed it in turbulent fire simulations and found it can yield better results. So here, τ_{mix} is expressed as

$$\tau_{mix} = \sqrt{\left(\frac{\nu}{\varepsilon}\right)^{0.5} \cdot \frac{k}{\varepsilon}} \tag{13}$$

where ν is the kinematic viscosity coefficient. k and ε are total turbulent kinetic energy and its dissipation rate in the LES framework.

In this paper, the Eddy-Dissipation-Concept (EDC) Model was employed to account for combustion rate calculation. It was originally developed by Magnussen et al. [33, 34], and recently extended to LES by Chen et al. [19,20] and further modified by Wang et al. [35] to handle multi-component fuels. Just like PaSR, EDC also splits a computational cell into the reacting and non-reacting zones. The reacting zone in EDC is the reacting part of the fine structure while the non-reacting zone is the combination of the non-reacting part of fine structure and surrounding fluid zone. Magnussen [37] suggested that soot could be produced not only in the fine structures but also surrounding fluids since its formation is relatively slow in comparison to gaseous combustion. Therefore in each computational cell, the reacting and non-reacting zones for soot are different from that for combustion in the EDC context. Since gas combustion is much faster than soot chemistry and the latter has relatively little influence on flame temperature and other field parameters like $\hat{\mathrm{Y}}_{\mathrm{fu}}$, $\hat{\mathrm{Y}}_{02}$, $\hat{T}$ and $\hat{\rho}$ in formula (9), it is therefore feasible to use the average values between the fine structure and surrounding fluid calculated by the EDC model for soot computations. It should also be noted that these parameters, especially temperature, are computed before heat transfer between different cells is solved. Moreover, they are also significantly different from or higher than the filtered and Favre- averaged values.

$$\hat{T} = T^{*}\gamma^{*}\chi + T_{Sur}\left(1-\gamma^{*}\chi\right) \tag{14}$$

$$\hat{\mathrm{Y}} = Y^{*}\gamma^{*}\chi + Y_{Sur}\left(1-\gamma^{*}\chi\right) \tag{15}$$

$$\hat{\mathrm{Z}} = \frac{\left(\frac{2\hat{\mathrm{Y}}_{\mathrm{c}}}{\mathrm{W}_{\mathrm{c}}} + \frac{\hat{\mathrm{Y}}_{\mathrm{H}}}{2\mathrm{W}_{\mathrm{H}}}\right)_{\mathrm{F}} + \frac{\hat{\mathrm{Y}}_{\mathrm{O}}^{\infty}}{\mathrm{W}_{\mathrm{O}}}}{\left(\frac{2\hat{\mathrm{Y}}_{\mathrm{C}}^{\mathrm{I}}}{\mathrm{W}_{\mathrm{c}}} + \frac{\hat{\mathrm{Y}}_{\mathrm{H}}^{\mathrm{I}}}{2\mathrm{W}_{\mathrm{H}}}\right)_{\mathrm{F}} + \frac{\hat{\mathrm{Y}}_{\mathrm{O}}^{\infty}}{\mathrm{W}_{\mathrm{O}}}} \tag{16}$$

$$\hat{\rho} = \frac{\bar{p}}{R\hat{T}} \tag{17}$$

where $\hat{Y}_k$ and W_k are the elemental mass fraction and atomic weight for element k; Superscripts I and ∞ refer to values at the inlet and ambient condition, respectively; Superscripts C, H, O are carbon, hydrogen and oxygen. Subscript F denotes fuel stream; $\overline{p}$ is Favre- averaged pressure. T^* and Y^* are temperature and species mass fraction in fine structures while T_{Sur} and Y_{Sur} are those in surround fluid. γ^* and χ are mass fraction and reacting fraction of the fine structures, respectively. To calculate these parameters in EDC, please refer to [37, 24, 25].

3. Numerical Setup

The above modifications were implemented into an in-house version of the FireFOAM code [24-25]. The equations for continuity, species mass fraction, momentum, sensible enthalpy and soot mass fraction are solved implicitly using the finite volume method. The time term is discretized using the backward time scheme with second order accuracy, and the limited central differencing scheme with second order accuracy is used to discretise the convection term. The diffusion term and gradient term are evaluated by the central differencing scheme. The finite volume discrete ordinates model (fvDOM) was employed to resolve the radiative heat transfer equation. The total absorption coefficient is calculated as the sum of the component gas absorption coefficient by the Weighted-Sum-of-Gray-Gases Model [39,40], and soot absorption coefficient computed following Chatterjee et al. [23], $\kappa_s \approx 1226 f_v T$,where f_v denotes soot volume fraction.

For validation, the 30 cm diameter heptane and toluene pool fires tested by Klassen and Gore [29] are simulated. The computational domain is a cylinder 2 m in diameter and 4 m high. Preliminary tests have shown that such a domain size is sufficiently large to avoid the influence of boundary effects on the pool fire development. Non-uniform grids are used with finer mesh clustered around the pool. The feeding rates for heptane and toluene are calculated as 2.559g/s and 3.05 g/s from the mass burning rates in the experiment [29], giving a theoretical heat release rate of 115 kW and 125 kW, respectively. As

temperature on the liquid fuel surface is believed to be steady if the boiling point is reached due to the continuous radiation feedback from the flame, the inlet temperatures are set to the boiling points of heptane (372 K) and toluene (384 K), respectively. The laminar smoke point heights are set as 0.147 m and 0.008 m following Tewarson [41] for heptane and toluene.

Three different grid resolutions were applied with the cell number of 16, 24 and 32 across the diameter of the pool. In another measure, around 22, 33 and 45 cells are used for the characteristic plume length scale $D^* = \left(\frac{Q}{\rho_\infty C_p T_\infty \sqrt{g}} \right)^{2/5}$,where Q , C_p , ρ_∞ , T_∞ and g denote heat release rate, specific heat, ambient air density, ambient air temperature and gravity acceleration respectively. Comparison of the predictions with the three different grid resolutions will be provided for the centreline temperature distributions while the predictions with the medium grid resolution (24 cells across the pool) are used to prepare the plots.

4. Results and Discussions

4.1 Heptane Pool Fire

4.1.1 Temperature

Figure 1 presents the comparison of the predicted centreline mean temperature rise with the measurements of Klassen and Gore [29]. The x-coordinate is the normalised height against $Q^{2/5}$ following McCaffrey [42]. The continuous flame zone corresponds to $H/Q^{2/5} \le 0.08$ (or $H/D \le 1.8$) while the intermittent flame zone is in the region $0.08 \le H/Q^{2/5} \le 0.2$ (or $1.8 < H/D \le 4.45$). No significant difference was found between the final solutions produced by three grid resolutions. The predictions are in good agreement with the measurements of Klassen and Gore [29] in the continuous and intermittent flame zones. Only when $H/Q^{2/5}$ is close to 0.2, the predictions differ considerably with the experimental data. The latter shows much steeper drop. As commented by Klassen and Gore [29], the temperature was measured based on the light intensities at two wavelengths. Close to the end of the

flame intermittent zone, the measured temperatures exhibited a relatively large fluctuation, which caused some uncertainty in the measurements. This disagreement may be also partly attributed to the numerical models.

Figure 2 presents mean temperature rise along the centerline predicted by the current model and that of Chen et al. [24, 25]. The predictions are generally very close, only when $H/Q^{2/5}$ falls within the range of 0.08~0.2, the current model predicted slightly higher temperature than that of Chen et al. [24, 25]. The maximum discrepancy is around 66K. This implies that the current model predicts a higher temperature in the intermittent flame zone.

Figure 3 presents the comparison between the predicted and measured mean temperature distributions at five different heights along the radial direction. The predicted mean temperature profile follows well the trend of the measurements. At H/D=0.9 and 1.5, the temperature near the centreline is well predicted but considerable discrepancies are observed in the outer region or 0.04m away from the burner centreline. At H/D=2.2 and 3.4, the predicted temperature profiles agree well with the measurements. With further increase of height, e.g. at H/D=4.3, the temperature is over-predicted. Since this height corresponds to the intermittent flame region, the actual flame in this region was observed to sway transversely, causing the averaged flame area wider than the experimental and the temperature measurements being somehow smeared [29]. Comparing the results predicted by both models, just like the centerline temperature, the current model predicts slightly higher temperature than that of Chen et al. [24, 25]. The discrepancy is more significant for the higher regions with $H/D \geqslant 2.2$.

It is, however, encouraging to note that in the main soot formation zone or near the centreline, the temperature is predicted with reasonably good accuracy.

4.1.2 Soot Volume Fraction

Figure 4 presents mean soot volume fractions along the centreline as a function of normalized height for the heptane pool fire, predicted by the current and Chen et al.'s [24, 25] models. It is found

that, for $H/Q^{2/5} \le 0.054\,m/kW^{1/5}$, the current model predicted higher soot volume fraction than that of Chen et al. [24, 25] , and the maximum ratio of soot volume fraction predicted by the two models is about 1.9. The inverse trend can be observed with the maximum discrepancy of 9.6% for $H/Q^{2/5} > 0.054 m/kW^{1/5}$.

Figure 5 presents the predicted soot volume fractions in the radial direction at different heights together with the measurements. The predictions are in reasonably good agreement with the experimental data. A relatively large discrepancy is observed near the centreline at H/D=0.9. The predicted value ranges from 0.4 ppm to 0.6 ppm while the measured value is around 0.6~0.8 ppm. This is opposite to the temperature predictions at the same height as shown in Fig.3, where the temperature near the centreline is well predicted but considerable discrepancies are seen in the outer region. This implies that soot formation and oxidation are not only affected by the temperature but also the local turbulence; and the latter evidently plays a dominant role. As shown in eqs. (10) , (11) and (13), turbulent mixing determines firstly the turbulence mixing time and then the mass fractions of the reacting part for soot formation and oxidation in each cell. For pool fires, the actual turbulence is relatively weak close to the burner surface in the persistent flame region. So the turbulence mixing time near the centreline at H/D=0.9 is over predicted. This is thought to be the main reason for the discrepancy in the predictions of the soot volume fraction near the pool surface.

As discussed above, with the increase of H/D, the current model predicts slightly higher temperature than that of Chen et al. [24, 25]. But for the soot volume fractions, this trend cannot be observed. For H/D $\geqslant$1.5, both models predicted nearly the same soot volume fractions. However, for H/D=0.9, the predicted soot volume fraction by the current model is closer to the measured data than that of Chen et al. [24, 25].

4.1.3 Soot formation and oxidation rates

Figure 6 presents soot formation and oxidation rates in the reacting parts along the centreline predicted by the current model and that of Chen et al. [24, 25] for the heptane pool fire. Both models predicted nearly identical soot formation rates in the reacting parts except some small differences near the peaks. But for soot oxidation rates in the reacting parts, Chen et al. predicted much larger rate than the current model due to its assumption of infinite soot oxidation.

Figure 7 presents turbulent soot formation and oxidation rates predicted by the two models. Even though a large discrepancy is shown in the laminar parts of the oxidation rates, the predictions of the two models are quite close. This is thought to be due to the fact that Chen et al. [24, 25] used the EDC concept to compensate the discrepancy due to the assumption of infinite laminar soot formation rate, by the following formula

$$\overline{\omega}_{S,O} = \begin{cases} \dfrac{\overline{\rho}\widetilde{Y}_S \dot{m}^* \gamma^* \chi}{1-\gamma^* \chi} & 0 \le \mathrm{Z} \le \mathrm{Z_{S,O}} \text{ and } \mathrm{T} \ge 1300\ \mathrm{K} \\ 0 & \text{else} \end{cases} \tag{18}$$

where $\dot{m}^*$ is mass transfer per unit of mass of the fine structure region.

4.1.4 Characteristic time scales

Figure 8 presents the contours of τ_{mix}, $\tau_{S,f,c}$ and $\tau_{S,O,c}$ for heptane pool fire. The characteristic time for turbulent mixing τ_{mix} falls in the range of 0~10 s. According to this, the flow fields of $\tau_{S,f,c}$ and $\tau_{S,O,c}$ are scaled to 0~100 s, as shown in Figure 8(b) and (c). It is found that both $\tau_{S,f,c}$ and $\tau_{S,O,c}$, which has the same order as or one order higher than τ_{mix}, fall in the regions of fire plume boundary and fire surface. Actually only $\tau_{S,f,c}$ and $\tau_{S,O,c}$ in fire surface can contribute to the soot formation and oxidation due to enough high temperature. So the limited region can be available for soot formation and oxidation.

4.2Toluene Pool Fire

4.2.1 Temperature

Figure 9 presents the comparison of the predicted centreline mean temperature rise with the measurements of Klassen and Gore [29] for the toluene pool fire. Similar to the case of the heptane pool fire, the predictions of the three grid resolutions are nearly the same and in good agreement with the measurements of Klassen and Gore [29] in the continuous and intermittent flame zones. But when $H/Q^{2/5}$ is close to 0.2, the predictions are slightly higher than the experimental data.

Figure 10 presents mean temperature rise alone the centreline, predicted by the current model and that of Chen et al. [24, 25]. The results are generally very close except for the region of $H/Q^{2/5} > 0.1$, the current model predicted slightly higher temperature than their model with the largest discrepancy being around 89 K.

Figure 11 shows the comparison between the predicted and measured temperature profiles in the radial direction at different heights. The predicted temperature profiles show similar trends as the measurements. However, the model over-predicted the temperatures away from the centreline at every examined height. It is thought that this is mainly caused by some known uncertainties in the experimental measurements although model assumptions might also have contributed to some degree. In the experiment, as reported by Klassen and Gore[29], the time-averaged flame height was measured as 1.30 m, indicating that the position of H/D=4.3 (equivalent to H=1.29 m) would roughly correspond to the position of the flame tip or in the intermittent flame region. This cast doubt on the measured temperature of 450 K near the centreline at H/D=4.3, implying the existence of considerable uncertainty in the temperature measurements or significant heat loss from the flame to the environment which was not described in the paper.

4.2.2 Soot Volume Fraction

Figure 12 presents mean soot volume fractions along the centreline vs. normalized height for the toluene pool fire, predicted by current model and Chen et al.'s[24, 25]. Compared with heptane pool fire, similar variation trend of soot volume fractions by two models can be observed for toluene pool fire. However, $H/Q^{2/5}$ at the first cross point is shifted from $0.054 m/kW^{1/5}$ to $0.057\ m/kW^{1/5}$. The maximum ratio of soot volume fraction by two models is about 8 for $H/Q^{2/5} \le 0.057\ m/kW^{1/5}$ while it is around 1.2 for $H/Q^{2/5} > 0.057 m/kW^{1/5}$.

Figure 13 presents the predicted and measured soot volume fractions along the radial direction at different heights by the two models. Generally, the predictions of the current model are in reasonable agreement with the measurements. However, at H/D=0.8 and 2.3, the model under-predicted the soot volume fraction near the centreline. As discussed earlier for the case of the heptane fire, the predicted turbulence mixing time is significantly lower than the experimental one. But in the outer region with distance more than 0.04m from the burner centreline, the model performed well. The predictions of the model of Chen et al. [24, 25] are close to the current model for each H/D.

4.2.3 Soot formation and oxidation rates

Figure 14 presents laminar parts of soot formation and oxidation rates predicted by the two models. It is easily observed that both models predicted nearly the identical laminar part of soot formation rate. However, for the laminar parts of soot oxidation rate, the predictions of Chen et al. [24, 25] are more than an order of magnitude larger than that of the current model. As discussed earlier for the case of the heptane fire, this discrepancy is attributed to the assumption of infinite laminar soot oxidation rate in the model of Chen et al. [24, 25].

Figure 15 presents the turbulent soot formation and oxidation rates predicted by the two models. As for the heptane fire, both models predicted nearly the same turbulent soot formation and oxidation rates, but the model of Chen et al. [24, 25] predicted slightly larger peak for the soot formation rate and

smaller peak for the oxidation rate. The largest discrepancies for the predicted turbulent soot formation and oxidation rates by the two models are about 24% and 37%, respectively.

4.2.4 Characteristic time scales

Figure 16 presents the contours of τ_{mix}, $\tau_{S,f,c}$ and $\tau_{S,O,c}$ for toluene pool fire. Similar to heptane pool fire, both $\tau_{S,f,c}$ and $\tau_{S,O,c}$ in toluene pool fire, which has the same order as or one order higher than τ_{mix}, also fall in the regions of fire plume boundary and fire surface. For both heptane and toluene pool fires, it is easy to be deduced that C_{SP} is not a constant and moreover varies with space location.

5. Conclusions

The extension of the laminar smoke point based approach to turbulent combustion using the partially stirred reactor (PaSR) concept proposed by Chen et al. [24, 25] has been modified to overcome the limitation associated with the assumption of infinitely fast soot oxidation chemistry and constant soot formation characteristic time. The mass fractions of the reacting zone in each cell for soot formation $\kappa_{s,f}$ and oxidation $\kappa_{s,o}$ are introduced. Both soot formation and oxidation are considered as taking place at finite rates while $\kappa_{s,f}$ and $\kappa_{s,o}$ are recomputed from the turbulence characteristic time and the newly introduced soot formation and oxidation characteristic time based on time-and-space dependent parameters. The governing equations have been modified to take into account both soot formation and oxidiation rates. The average parameters between the fine structure and surrounding fluid computed by the EDC are employed instead of those Favre-averaged values in soot formation model [24, 25]. All these modifications have been implemented into the FireFOAM code for testing within a CFD environement.

For model validation, numerical simulations were conducted for the 30 cm diameter heptane and toluene pool fires tested by Klassen and Gore [29]. Reasonably good agreement has been achieved between the predicted and measured soot volume fractions in both cases while relatively large

discrepancies are seen for the recorded height in the persistent flame zone close to the pool centerline. The predicted temperature distributions along the centreline and the radial directions at different heights for the heptane fire are found to be in good agreement with the measurements. The temperature predictions for the toluene pool fire are found to be generally higher than the measurements but the decrepancies are likely to be mainly caused by the known uncertainties in the measurements[29] with some contributions from the model. The characterisitic times for soot formation and oxidation, which has the same order as or one order higher than the characterisitic time for turbulent mixing , fall in the regions of fire plume boundary and fire surface.

In comparison with the previously developed soot model of Chen et al. [24, 25], the predictions of the current model for soot formation and oxidition rates are closer to the measurements for most cases, especially close to the fire base. However, there are no significant differences between the predictions of the two models for the heights and axis examined. A possible explanation is that despite the unphysical assumption of infinite rate of lamilar soot oxidation by Chen et al. [24, 25], their use of the EDC aproach to calculate soot oxidation has to some extent offset the discrepancy which could have been caused by this assumption. The present model is physically more sound. Further tests with different sets of data will be useful to formulate more conclusive recommendations but this is unfortunately hindered by the lack of soot measurements for pool fires.

Acknowledgements

The authors would like to acknowledge the return phase funding from the European Commission for the Marie Curie International Fellowships (Grant No. 909658). Drs Yi Wang and Prateep Chatterjee of FM Global and Dr John Hewson of Sandia National Laboratory are gratefully acknowledged for technical discussion. Dr Yi Wang, in particular, has also provided detailed comments during the development of the model and preparation of the manuscript.

References

[1] P. Joulain, The behavior of pool fires: State of the art and new insights, Symposium (International) on Combustion, 27(1998) 2691–2706.

[2] T. Steinhaus, S. Welch, R.O. Carvel, J.L. Torero, Large-scale pool fires. Thermal Science, 11 (2007)101–118.

[3] C.D. Argyropoulos, G.M. Sideris, M.N. Christolis, Z. Nivolianitou, N.C. Markatos, Modelling pollutants dispersion and plume rise from large hydrocarbon tank fires in neutrally stratified atmosphere. Atmos Environ, 44(2010)803–813.

[4] P.K. Raj. Large hydrocarbon fuel pool fires: Physical characteristics and thermal emission variations with height. J Hazard Mater, 140(2007)280–292.

[5] K.B. McGrattan, H.R. Baum, A. Hamins, Thermal radiation from large pool fires, Gaithersburg, USA, 2000, http://fire.nist.gov/bfrlpubs/fire00/PDF/f00177.pdf.

[6] M. Frenklach, D.W. Clary, W.C. Gardiner, S.E. Stein, Detailed Kinetic Modeling of Soot Formation in Shock-Tube Pyrolysis of Acetylene, Proc. Combust. Inst. 20 (1984) 887–901.

[7] H. Wang, M. Frenklach, A Detailed Kinetic Modeling Study of Aromatics Formation in Laminar Premixed Acetylene and Ethylene Flames, Combust. Flame 110 (1-2) (1997) 173–221.

[8] S. Li. Modeling of pressure effects on flame structure and soot formation of n-heptane/air co-flow laminar flames by skeletal reaction mechanism, Appl.Therm. Eng. 106 (2016) 1458 – 1465.

[9] A. D'Anna, A. D'Alessio, P. Minutolo, in: H.Bockhorn (Eds.), Soot Formation in Combustion: Mechanisms and Models, Springer-Verlag, Berlin, 1994, p. 83.

[10] J.H. Kent, D.R.Honnery,in: H.Bockhorn (Eds.), Soot Formation in Combustion: Mechanisms and Models, Springer-Verlag, Berlin, 1994,p. 199.

[11] J.H. Kent, D.R.Honnery, A soot formation rate map for a laminar ethylene diffusion flame, Combust.Flame 79 (1990) 287-298.

[12] J.B. Moss, C.D. Stewart, Flamelet-Based Smoke Properties for the Field Modelling of Fires, Fire Safety J30 (1998) 229-250.

[13] C.W. Lautenberger, N.A. Dembsey, J.L. de Ris, A. Dembsey, J.R. Barnett, H.R. Baum, A Simplified Model for Soot Formation and Oxidation in Cfd Simulation of Non-Premixed Hydrocarbon Flames, Fire Safety J. 40 (2005) 141–176.

[14] G.H.Markstein, J.L. De Ris, Radiant Emission and Absorption by Laminar Ethylene and Propylene Diffusion Flames, Proc. Combust. Inst. 20 (1985) 1637-1646.

[15] M.A. Delichatsios, A phenomenological model for smoke-point and soot formation in laminar flames, Combust Sci. Technol.100 (1994) 283–298.

[16] C.W. Lautenberger, *CFD* Simulation of Soot formation and Flame Radiation, Master Thesis, Worcester Polytechnic Institute, Worcester, MA, 2002.

[17] T. Beji, J. Zhang, M.A. Delichatsios, Determination of soot formation rate from Laminar Smoke Point measurements, Combust Sci. Technol. 180 (5) (2008) 927–940.

[18] T. Beji, J. Zhang, W. Yao, M.A. Delichatsios, A novel soot model for fires: Validation in a laminar non-premixed flame, Combust.Flame 158 (2011) 281-290.

[19] W. Yao, J. Zhang, A Nadjai, T. Beji, M.A. Delichatsios, A global soot model developed for fires: Validation in laminar flames and application in turbulent pool fires, Fire safety J. 46 (2011)371-387.

[20] R.P. Lindstedt, Simplified soot nucleation and surface growth steps for non- premixed flames, Soot Formation in Combustion: Mechanisms and Models, Springer-Verlag Series in Chemical Physics, vol. 59, Springer Verlag, Berlin, 1994, pp. 417–441.

[21] K.M. Leung, R.P. Lindstedt,W.P. Jones, A Simplified Reaction Mechanism for Soot Formation in Nonpremixed Flames, Combust. Flame 87 (1991) 289–305.

[22] W. Yao, J. Zhang, A Nadjai, T. Beji, M.A. Delichatsios, Development and Validation of a Global Soot Model in Turbulent Jet Flames, Combust Sci. Technol. 184 (5) (2012) 717–733.

[23] P.Chatterjee, J.L. de Ris, Y. Wang, S.B. Dorofeev, A model for soot radiation in buoyant diffusion flames, Proc. Combus. Inst. 33(2)(2011) 2665-2671.

[24] Z.B. Chen, J. Wen, B.P. Xu, S. Dembele, Large eddy simulation of a medium-scale methanol pool fire using the extended eddy dissipation concept, Int. J of Heat and Mass Transfer, 70(2014)389-408.

[25] Z.B. Chen, J. Wen, B.P. Xu, S. Dembele, Extension of the eddy dissipation concept and smoke point soot model to the LES frame for fire simulations, Fire Safety J., 64 (2014) 12-26.

[26]B.K. Lee, W.M. Thring, M.J. Beer, On the rate of combustion of soot in a laminar soot flame, Comb ust. Flame 6 (1962) 137–145.

[27]Y.Wang, P.Chatterjee, J. L.de Ris, Large eddy simulation of fire plumes, Proc. Combust. Inst. 33(2011) 2473-2480.

[28]H.G.Weller, G.Tabor, H.Jasak, C.Fureby, A tensorial approach to computational continuum mechanics using object oriented techniques, Computers in Physics 12 (1998) 620-631.

[29]M.Klassen, J. Gore, Structure and Radiation Properties of Pool Fires, Report No. NIST-GCR-94-651, National Institute of Standards and Technology, 1992.

[30]N.Nordin, Complex Chemistry Modeling of Diesel Spray Combustion, PhD thesis, Chalmers University of Technology, Gothenburg, Sweden, 2001.

[31]J.Chomiak, A. Karlsson, Flame liftoff in diesel sprays, Proc. Combust. Inst. 26(2) (1996) 2557-2564.

[32]F.Tao, V.I. Golovitchev, J. Chomiak, A phenomenological model for the prediction of soot formation in diesel spray combustion, Combust. Flame 136 (2004) 270-282.

[33]Smooke MD, Long MB, Connelly BC, Colket MB, Hall RJ, Soot formation in laminar diffusion flames, Combust. Flame 143(2005) 613-28.

[34]J.A.J. Karlsson, *Modeling* Auto-Ignition, Flame Propagation and Combustion in Non-stationary Turbulent Sprays. PhD thesis, Chalmers University of Technology, Göteborg,1995.

[35] J.A.J. Karlsson, J. Chomiak, Physical and Chemical Effects in Diesel Spray Ignition, 21st Congress of CIMAC, Interlaken Switzerland, May 15-18,1995

[36]B.F.Magnussen, B.Hjertager, On mathematical modeling of turbulent combustion with special emphasis on soot formation and combustion, Proc. Combust. Inst.16(1976) 719-729.

[37] B.F.Magnussen, The Eddy Dissipation Concept: A Bridge Between Science and Technology, Thematic Conference on Computational Combustion, Lisbon, Portugal. p. 1-25.

[38]C.J. Wang, J. Wen, Z.B. Chen, and S. Dembele, Predicting radiative characteristics of hydrogen and hydrogen/methane jet fires using FireFOAM. Int. J Hydrogen Energ. 39(2014) 20560-20569.

[39]T. F.Smith, Z. F.Shen, J. N.Friedman, Evaluation of coefficients for the weighted sum of gray gases model, J. Heat Transfer 104 (1982) 602-608.

[40]A.Coppalle, P.Vervisch, The total emissivities of high-temperature flames, Combust. Flame 49 (1983) 101-108.

[41]A. Tewarson, Smoke point height and fire properties of materials, Report No. NIST-GCR-88-555, National Institute of Standards Technology, 1988.

[42] McCaffrey B, Purely buoyant diffusion flames: Some Experimental Results, 1979.

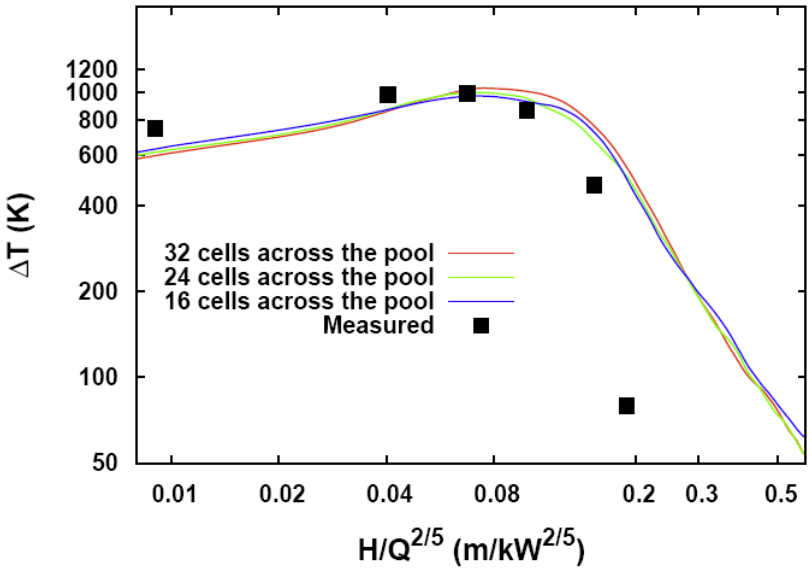

Fig.1 Mean temperature rise along the centreline *vs* normalized height for the heptane pool fire.

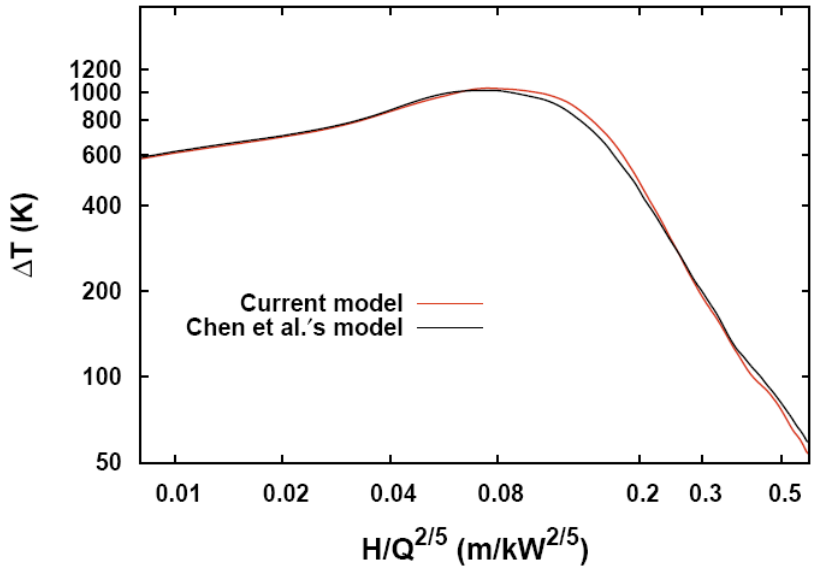

Fig.2 Mean temperature rise along the centreline *vs* normalized height for the heptane pool fire, predicted by the current and Chen et al.'s [24, 25] models.

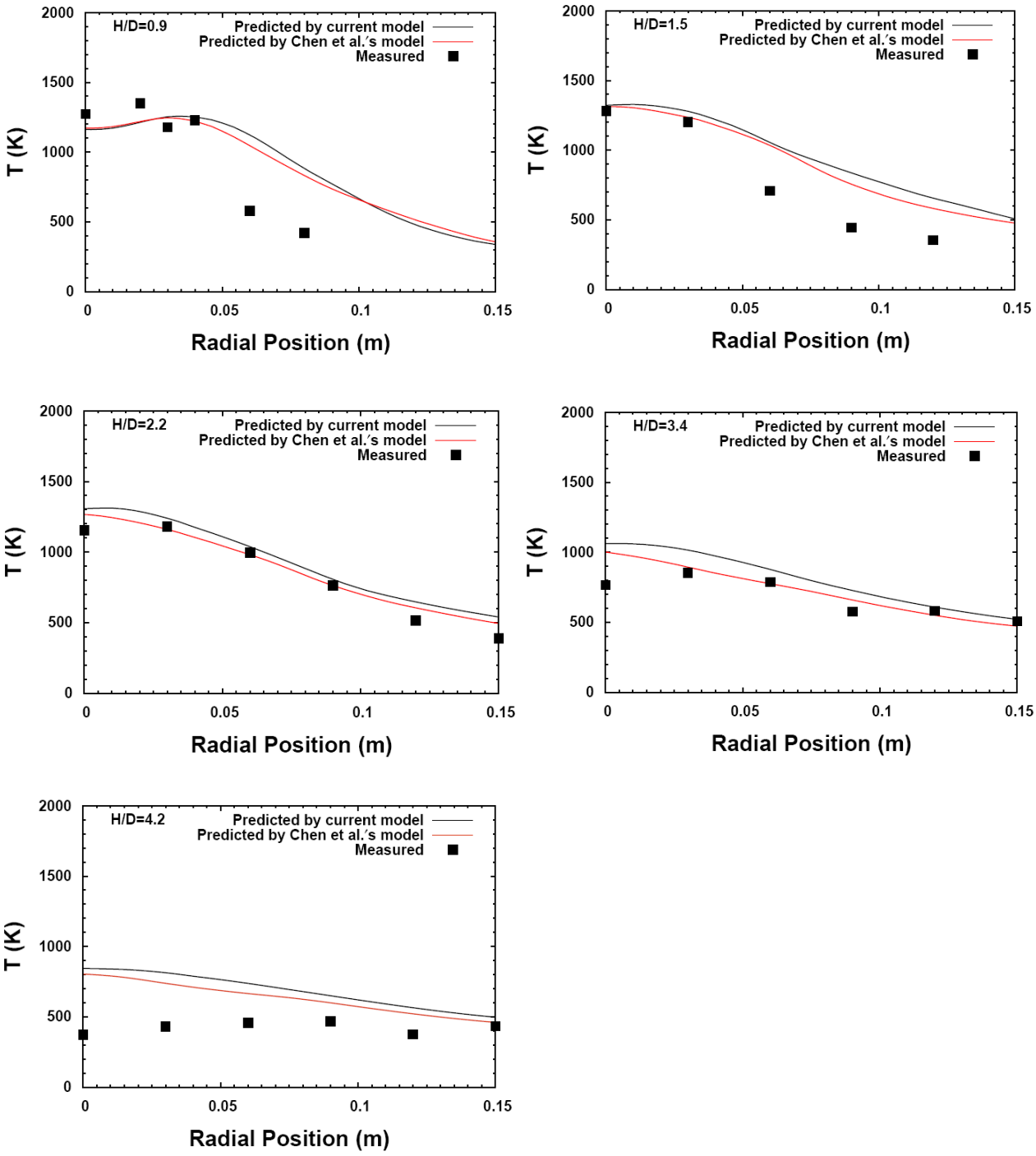

Fig.3 Comparison between the predicted and measured temperature profiles in the radial direction at different heights for the heptane pool fire.

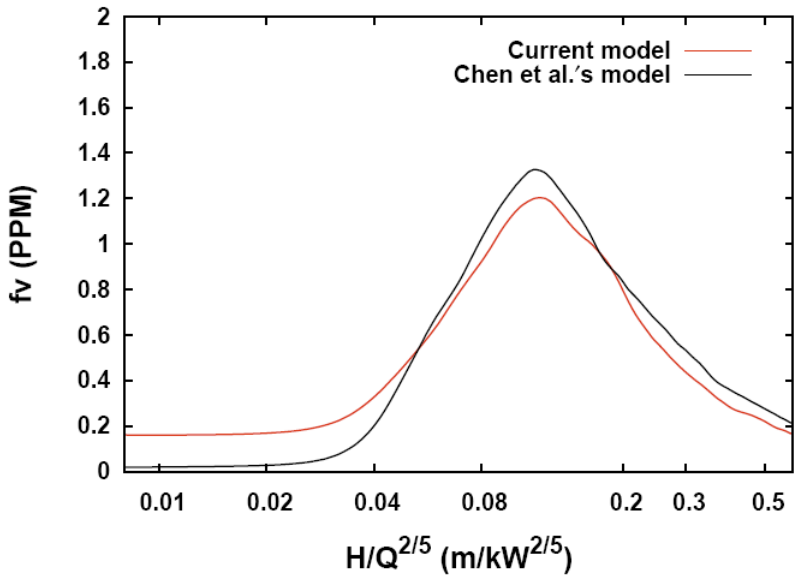

Fig.4 Mean soot volume fractions along the centreline *vs* normalized height for the heptane pool fire, predicted by the current and Chen et al.'s [24, 25] models.

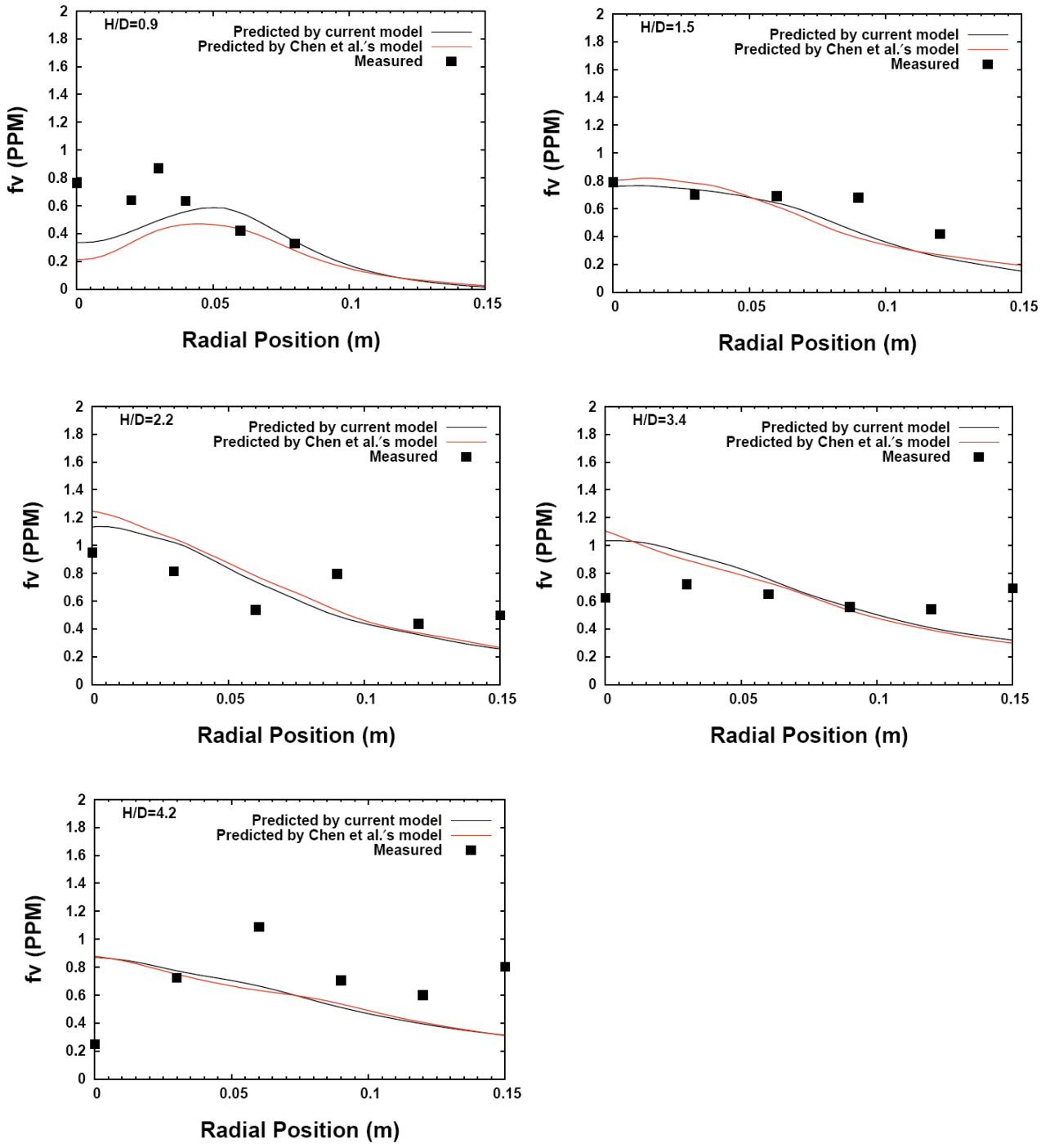

Fig.5 Comparison between predicted and measured soot volume fractions in the radial direction at different heights for the heptane pool fire.

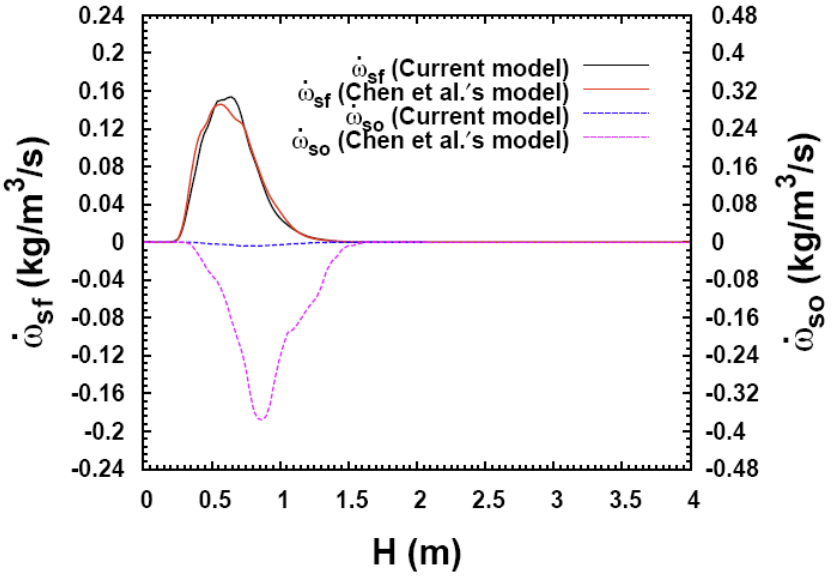

Fig.6 Soot formation and oxidation rates in the reacting parts along the centreline predicted by the current and Chen et al.'s [24, 25] models for the heptane pool fire.

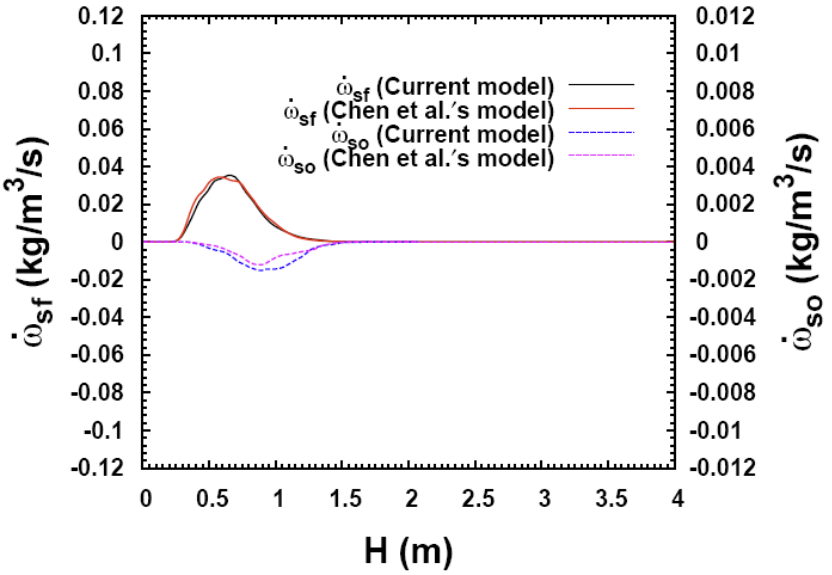

Fig.7 Turbulent soot formation and oxidation rates along the centreline predicted by the current and Chen et al.'s [24, 25] models for the heptane pool fire.

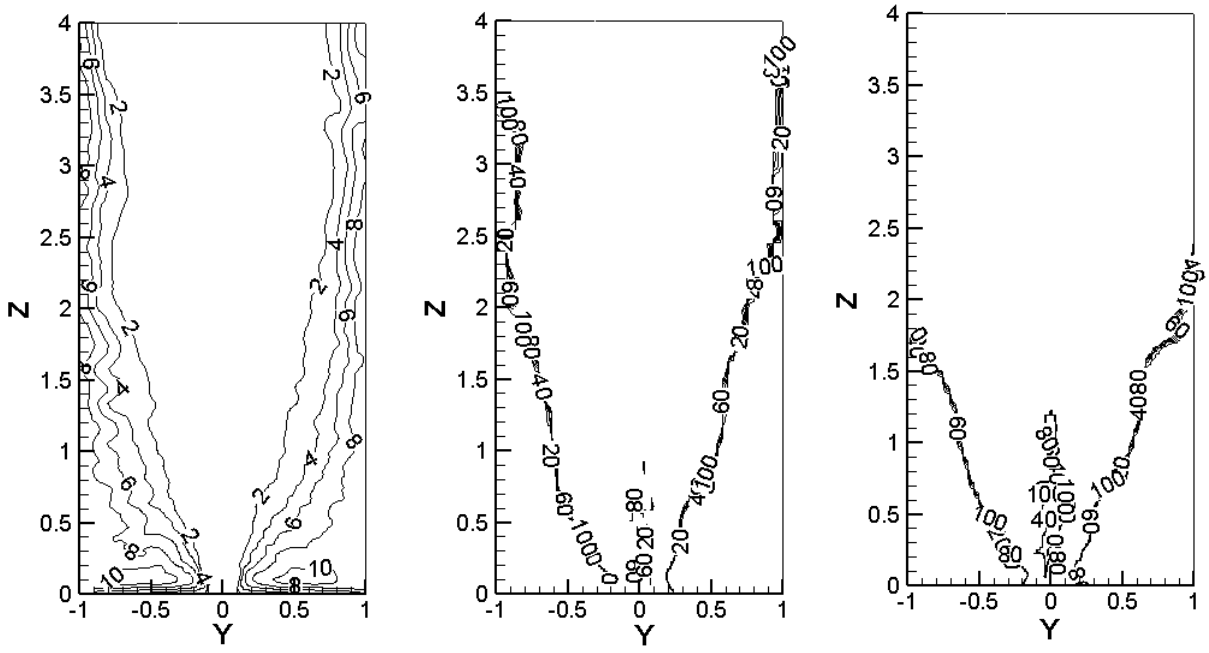

(a) τ_{mix} (b) $\tau_{S,f,c}$ (c) $\tau_{S,O,c}$

Fig.8 Characteristic time scales for the heptane pool fire.

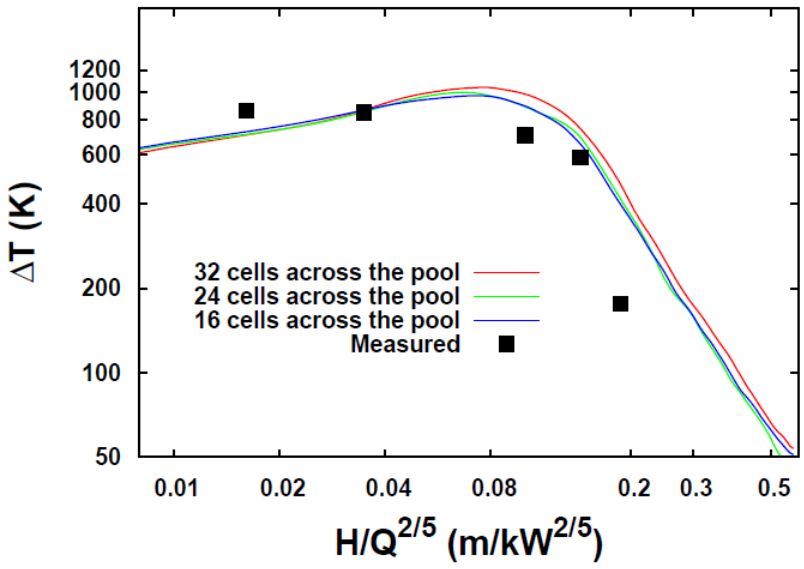

Fig.9 Mean temperature rise along the centreline *vs* normalized height for the toluene pool fire.

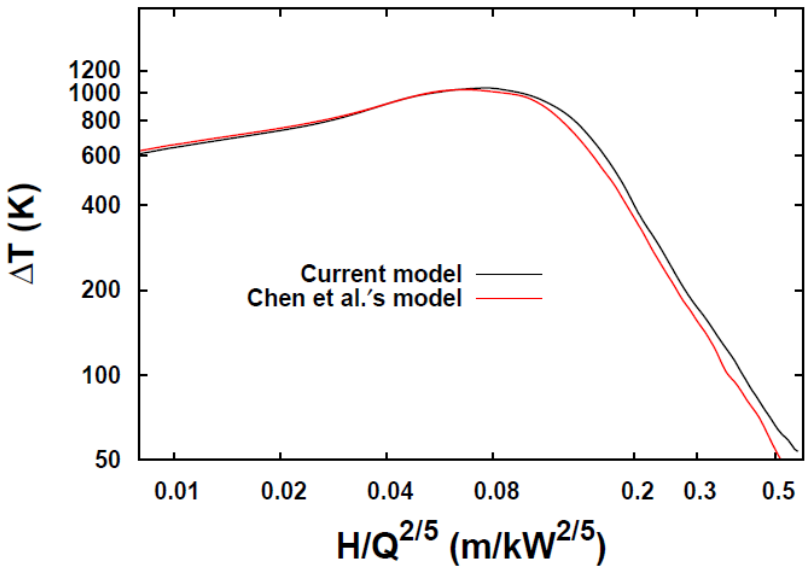

Fig.10 Mean temperature rise along the centreline *vs* normalized height for the toluene pool fire, predicted by current model and Chen et al.'s[24, 25].

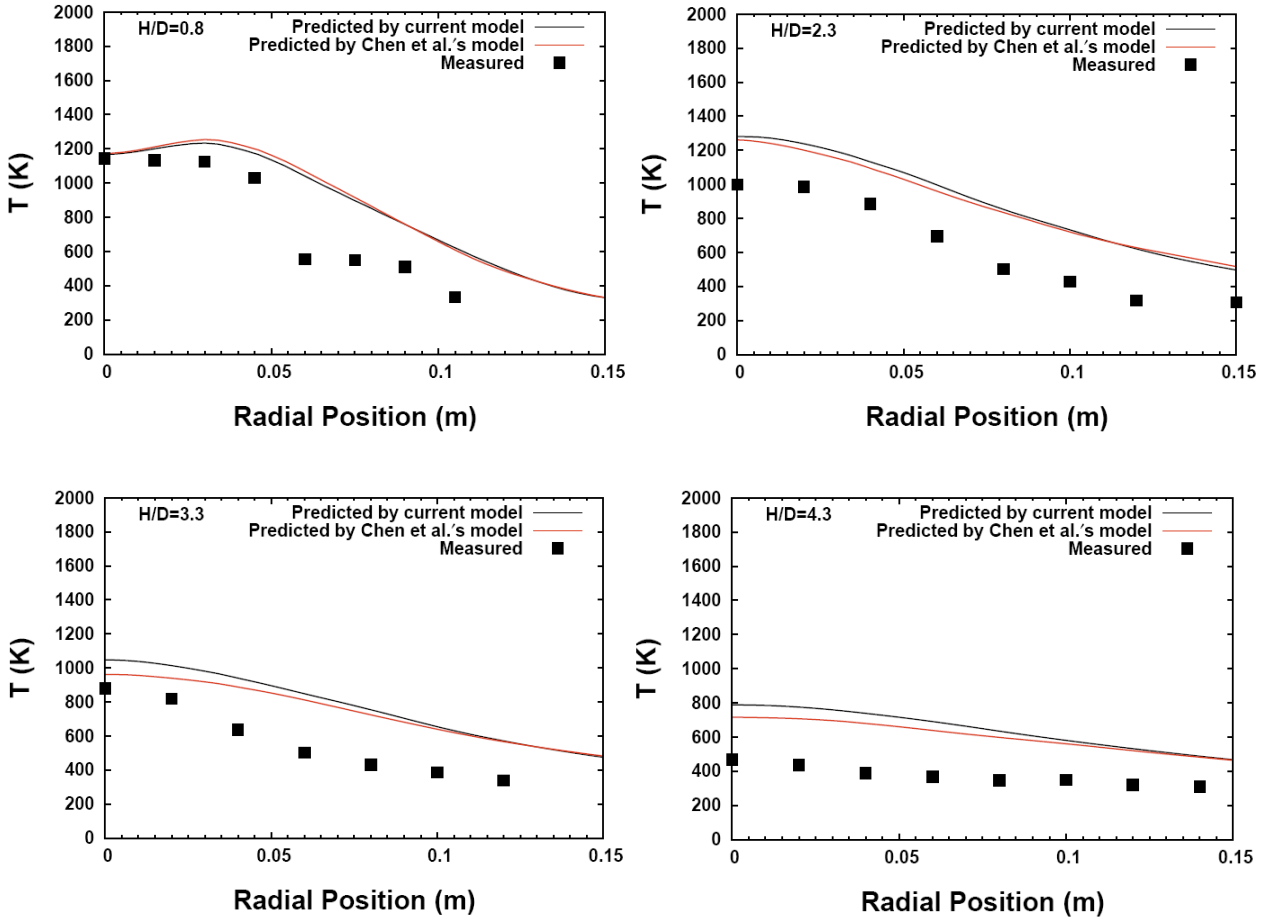

Fig.11 Comparison between predicted and measured temperature profiles in the radial direction at different heights for the toluene pool fire.

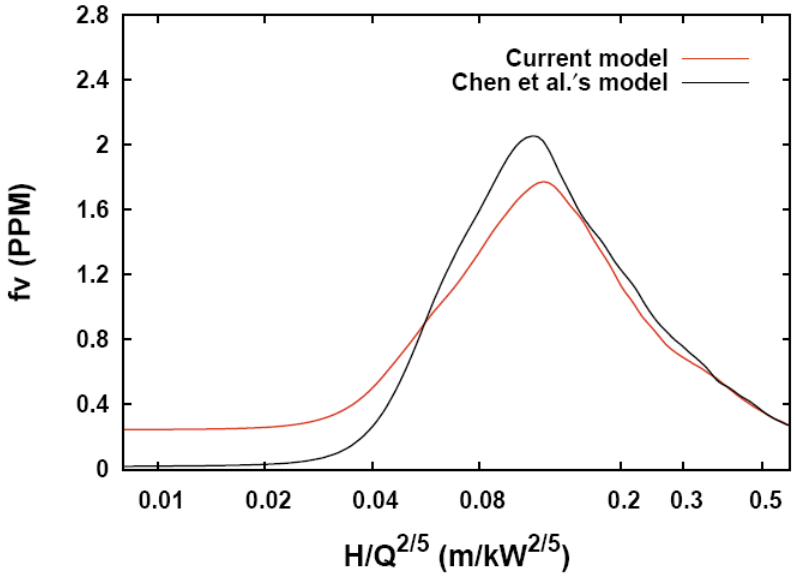

Fig.12 Mean soot volume fractions along the centreline *vs* normalized height for the toluene pool fire, predicted by current and Chen et al.'s [24, 25] models.

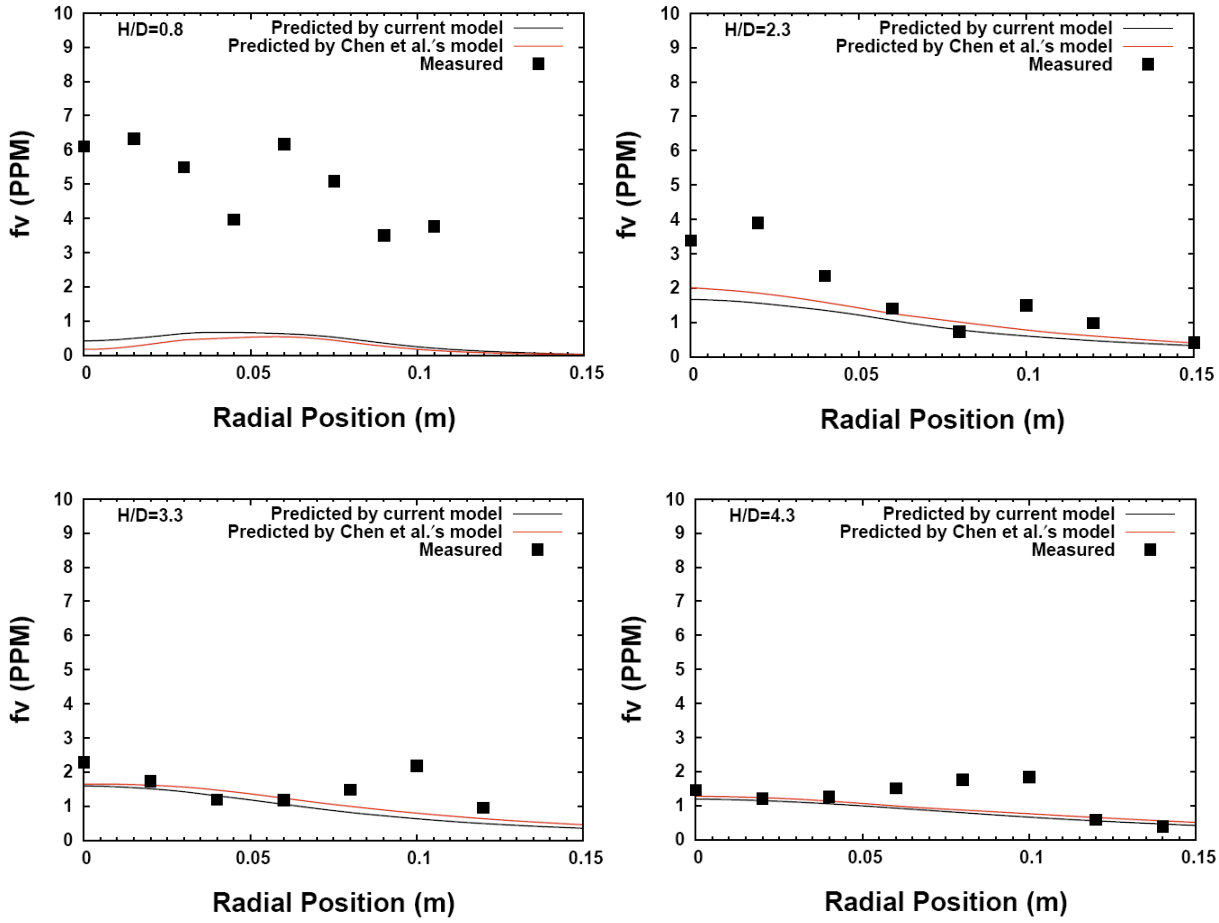

Fig.13 Comparison between the predicted and measured soot volume fractions in the radial direction at different heights for the toluene pool fire.

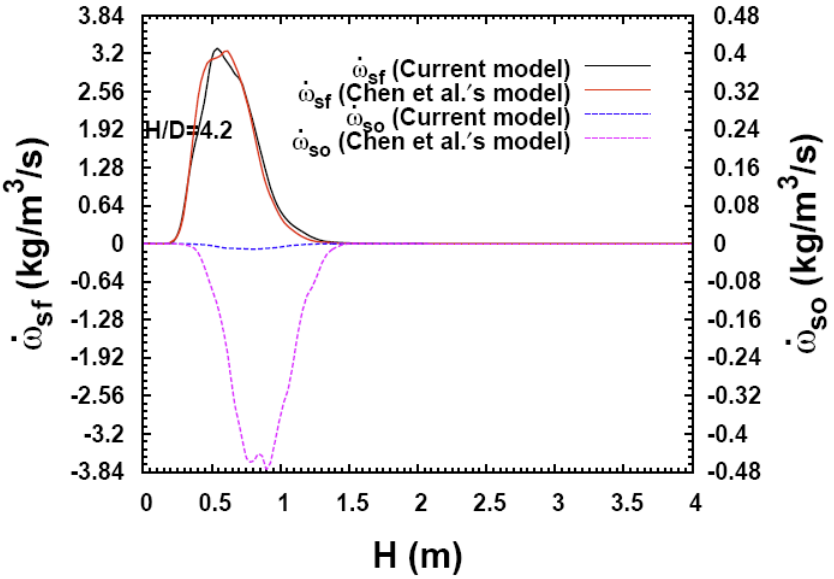

Fig.14 Soot formation and oxidation rates in the reacting part along the centreline predicted by the current and Chen et al.'s [24, 25] models for the toluene pool fire.

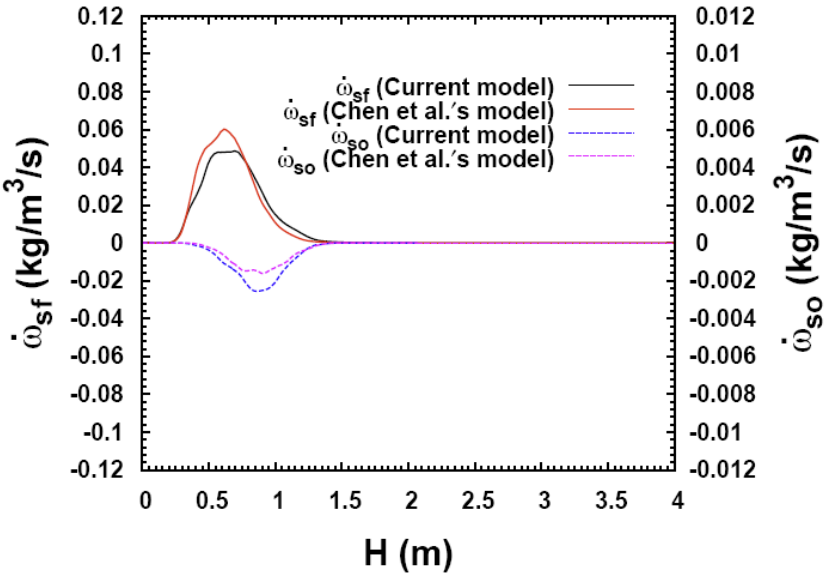

Fig.15 Turbulent soot formation and oxidation rates along the centreline predicted by the current and Chen et al.'s [24, 25] models for the toluene pool fire.

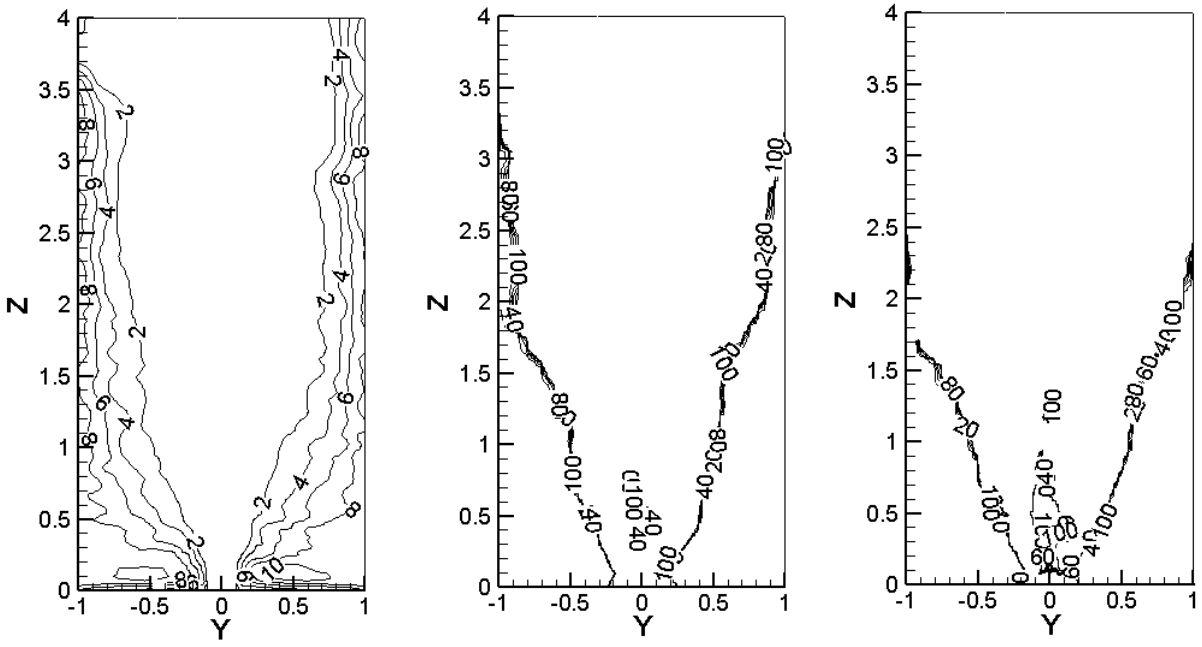

(a) τ_{mix} (b) $\tau_{S,f,c}$ (c) $\tau_{S,O,c}$

Fig.16 The predicted characteristic time scales for the toluene pool fire.

Figure Captions

Fig.1 Mean temperature rise along the centreline *vs* normalized height for the heptane pool fire.

Fig.2 Mean temperature rise along the centreline *vs* normalized height for the heptane pool fire, predicted by the current and Chen et al.'s [24, 25] models.

Fig.3 Comparison between the predicted and measured temperature profiles in the radial direction at different heights for the heptane pool fire.

Fig.4 Mean soot volume fractions along the centreline *vs* normalized height for the heptane pool fire, predicted by the current and Chen et al.'s [24, 25] models.

Fig.5 Comparison between predicted and measured soot volume fractions in the radial direction at different heights for the heptane pool fire.

Fig.6 Soot formation and oxidation rates in the reacting parts along the centreline predicted by the current and Chen et al.'s [24, 25] models for the heptane pool fire.

Fig.7 Turbulent soot formation and oxidation rates along the centreline predicted by the current and Chen et al.'s [24, 25] models for the heptane pool fire.

Fig.8 Characteristic time scales for the heptane pool fire.

Fig.9 Mean temperature rise along the centreline *vs* normalized height for the toluene pool fire.

Fig.10 Mean temperature rise along the centreline *vs* normalized height for the toluene pool fire, predicted by current model and Chen et al.'s[24, 25].

Fig.11 Comparison between predicted and measured temperature profiles in the radial direction at different heights for the toluene pool fire.

Fig.12 Mean soot volume fractions along the centreline *vs* normalized height for the toluene pool fire, predicted by current and Chen et al.'s [24, 25] models.

Fig.13 Comparison between the predicted and measured soot volume fractions in the radial direction at different heights for the toluene pool fire.

Fig.14 Soot formation and oxidation rates in the reacting part along the centreline predicted by the current and Chen et al.'s [24, 25] models for the toluene pool fire.

Fig.15 Turbulent soot formation and oxidation rates along the centreline predicted by the current and Chen et al.'s [24, 25] models for the toluene pool fire.

Fig.16 The predicted characteristic time scales for the toluene pool fire.